Qubit Measurement by Multichannel Driving

Joni Ikonen,[1] Jan Goetz,[1] Jesper Ilves,[1] Aarne Keränen,[1] Andras M. Gunyho,[1] Matti Partanen,[1] Kuan Y. Tan,[1] Dibyendu Hazra,[1] Leif Grönberg,[2] Visa Vesterinen,[1,2] Slawomir Simbierowicz,[2] Juha Hassel,[2] and Mikko Möttönen[1]

[1]*QCD Labs, QTF Centre of Excellence, Department of Applied Physics, Aalto University, P.O. Box 13500, FI-00076 Aalto, Finland*

[2]*VTT Technical Research Centre of Finland, QTF Center of Excellence, P.O. Box 1000, FI-02044 VTT, Finland*

(Received 5 October 2018; revised manuscript received 13 November 2018; published 25 February 2019)

We theoretically propose and experimentally implement a method of measuring a qubit by driving it close to the frequency of a dispersively coupled bosonic mode. The separation of the bosonic states corresponding to different qubit states begins essentially immediately at maximum rate, leading to a speedup in the measurement protocol. Also the bosonic mode can be simultaneously driven to optimize measurement speed and fidelity. We experimentally test this measurement protocol using a superconducting qubit coupled to a resonator mode. For a certain measurement time, we observe that the conventional dispersive readout yields close to 100% higher average measurement error than our protocol. Finally, we use an additional resonator drive to leave the resonator state to vacuum if the qubit is in the ground state during the measurement protocol. This suggests that the proposed measurement technique may become useful in unconditionally resetting the resonator to a vacuum state after the measurement pulse.

DOI: 10.1103/PhysRevLett.122.080503

Since the birth of quantum mechanics, quantum measurements and the related collapse of the wave function has puzzled scientists [1,2], culminating in various interpretations of quantum mechanics such as that of many worlds [3]. With the recent rise of quantum technology [4–6], the quantum measurement has become one of the most important assets for practical applications. For example, measurements of single qubits are the key in reading out the results of quantum computations [7–10] and parity measurements in multiqubit systems are frequently required in quantum error correction codes such as the surface and color codes [11–15]. Furthermore, single-qubit measurement and feedback can be used to reset qubits [16–18] or even solely provide the nonlinearity needed to implement multiqubit gates [19–21].

One of the most widespread ways to measure qubits is to couple them to one or several bosonic modes, such as those of the electromagnetic field, and to measure their effect on the radiation [22]. This method is currently used, for example, in quantum processors based on superconducting circuits [23–28], quantum dots [29–31], and trapped ions [32]. Especially with the rise of circuit quantum electrodynamics [33,34], this measurement technique has become available to many different hybrid systems such as mechanical oscillators [35,36] and magnons [37].

Theoretically, the interacting system of a qubit and a bosonic mode is surprisingly well described by the Jaynes–Cummings model [38,39]. If the qubit frequency is far detuned from the mode frequency, i.e., we operate in the dispersive regime, the interaction term renders the mode frequency to depend on the qubit state. Consequently, a straightforward way to implement a nondemolition measurement on the qubit state is to drive the mode at a certain frequency close to the resonance and measure the phase shift of the output field with respect to the driving field. This kind of dispersive measurement has been extremely successful, for example, in superconducting qubits [40] with increasing accuracy and speed [24,41–43] currently culminating in 99.2% fidelity in 88 ns [26].

In the dispersive measurement, one of the key issues has been the ability to quickly populate the bosonic mode in the beginning of the measurement protocol [24] without surpassing the critical photon number, and to quickly evacuate the excitations from the mode after the measurement [17,44]. These requirements point to the need for a fast, low-quality readout mode. However, this poses a trade-off on the qubit lifetime, which to some extent can be answered using Purcell filters [24,26,45] with the cost of added circuit complexity. A simple and fast high-fidelity measurement scheme is of great interest not only to the field of superconducting qubits, but also to other quantum technology platforms utilizing bosonic modes as the measurement tool.

Inspired by our recent work [46] on quickly stabilizing resonator states by a qubit drive, we propose in this Letter a qubit measurement protocol that is based on driving the qubit close to the frequency of the bosonic mode through a nonresonant channel. Owing to the dispersive coupling, the initial vacuum state of the resonator begins to rotate selectively on the qubit state about a point controlled by the strength and phase of the qubit drive. Importantly, this rotation begins immediately after the drive pulse arrives at

the qubit with no bandwidth limitation imposed by the resonator. We demonstrate this nondemolition readout scheme in planar superconducting qubits and observe that it leads to a significant speedup. Furthermore, we discuss how this method can be used to unconditionally reset the resonator state into vacuum after the readout without the need for feedback control. We experimentally demonstrate a related effect where the resonator is left in the vacuum state provided that the qubit was in the ground state.

Let us theoretically study a qubit coupled to a single bosonic mode such as that of an electromagnetic resonator, as shown in Fig. 1(a). Instead of using the conventional readout by populating the resonator with a coherent pulse [40,41], we measure the qubit state by driving the qubit at the resonator frequency ω_r. In addition, we can apply a compensation pulse to the resonator to eliminate cross-coupling effects with the qubit or otherwise control the resonator state. The qubit and the resonator couple to their respective driving fields with different strengths, which together with the pulse envelopes constitute the effective Rabi angular frequencies Ω_q and Ω_r, respectively. The qubit may be first excited from the ground state $|g\rangle$ to the excited state $|e\rangle$ by a separate drive tone at the transition angular frequency $\omega_q = \omega_r + \Delta$, where Δ is the detuning.

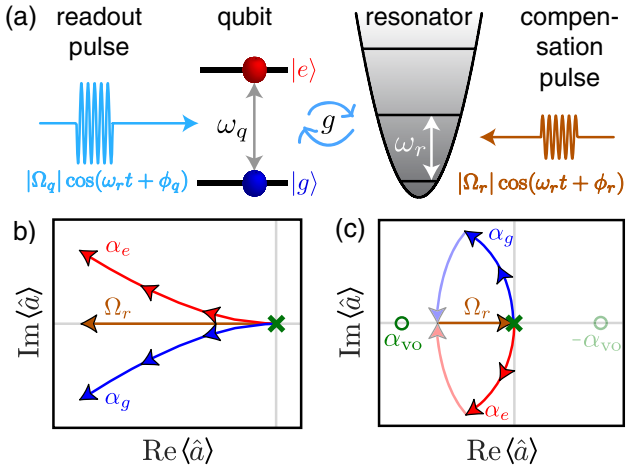

FIG. 1. (a) Schematic presentation of the readout scheme where the qubit is driven (blue color) at the frequency of a dispersively coupled bosonic mode. A compensation tone (brown color) on the resonator may be used to optimize the result. We consider the case where the detuning $\Delta = \omega_q - \omega_r$ is much greater than the qubit-mode coupling strength g. (b) Evolution of the mean of the resonator state in phase space for the conventional dispersive readout starting from vacuum (cross) provided that the qubit was prepared in $|g\rangle$ (blue) or $|e\rangle$ (red). (c) As (b) but the readout pulse is applied directly to the qubit. Thus, the resonator states start to rotate about a new virtual origin α_{vo} (circle) leading to a faster separation. After measurement, we may reverse the sign of the virtual origin and wait for the resonator states corresponding to different qubit states to fully overlap (faint colors). A subsequent shift (brown color) finalizes an unconditional reset of the resonator.

In the frame rotating at ω_r with respect to the bare qubit and resonator Hamiltonians, $\hbar\omega_q\hat{\sigma}_+\hat{\sigma}_-$ and $\hbar\omega_r\hat{a}^\dagger\hat{a}$, respectively, the system is described by the Jaynes–Cummings Hamiltonian

$$\hat{H}/\hbar = \Delta\hat{\sigma}_+\hat{\sigma}_- + (g\hat{\sigma}_+\hat{a} + \Omega_q\hat{\sigma}_+ + i\Omega_r\hat{a}^\dagger + \mathrm{H.c.}), \quad (1)$$

where g denotes the qubit-resonator coupling strength, $\hat{a}^\dagger$ and $\hat{\sigma}_+ \equiv |e\rangle\langle g|$ are the creation operators of the resonator mode and of the qubit, respectively. Above, we have introduced the rotating-wave approximation justified by $g \ll \omega_q, \omega_r$.

To demonstrate the benefit of driving the qubit at the frequency of the resonator, we employ the standard dispersive approximation [47] in the regime $g \ll |\Delta|$. This yields, up to constant energy terms, the Hamiltonian [48]

$$\hat{H}''/\hbar \approx (\Delta+\chi)\hat{\sigma}_+\hat{\sigma}_- + \left[\left(\Omega_q + i\Omega_r\frac{\chi}{g}\right)\hat{\sigma}_+ + \mathrm{H.c.}\right] - \chi\hat{\sigma}_z\hat{a}^\dagger\hat{a} + \left[\left(i\Omega_r - \Omega_q\frac{\chi}{g}\hat{\sigma}_z\right)\hat{a}^\dagger + \mathrm{H.c.}\right], \quad (2)$$

where $\chi = g^2/\Delta$ is the dispersive shift for a two-level system and $\hat{\sigma}_z = |g\rangle\langle g| - |e\rangle\langle e|$. The term proportional to $\hat{a}^\dagger$ is a generator of a displacement operator that depends on the state of the qubit. Thus, driving the qubit effectively realizes longitudinal coupling [56,57] for the duration of the readout, implying that the rate of state separation is not limited by the rate at which the resonator is populated.

In our work, the resonator is accurately described by a coherent state $|\alpha\rangle$ such that $\hat{a}|\alpha\rangle = \alpha|\alpha\rangle$, $\alpha \in \mathbb{C}$. The drive amplitude Ω_q may be turned on very fast, causing the amplitudes $\alpha_{g/e}$ corresponding to the eigenstates of the qubit, $|g\rangle$ and $|e\rangle$, to separate in the complex plane at least with the initial speed $2\Omega_q\chi/g$. This minimum speed is achieved with $\Omega_r = 0$ for an initial vacuum state in the resonator.

As the resonator becomes populated, the trajectories begin to curve due to the dispersive term $-\chi\hat{\sigma}_z\hat{a}^\dagger\hat{a}$ in Eq. (2) and, in fact, to rotate about the point $\alpha_{\mathrm{vo}} \equiv -\Omega_q/g$. This behavior is intuitively understood in a frame displaced by α_{vo}. Introducing a shifted annihilation operator $\hat{b} = \hat{a} - \alpha_{\mathrm{vo}}$, the last line of Eq. (2) yields

$$\hat{H}_r''/\hbar \approx -\chi\hat{\sigma}_z\hat{b}^\dagger\hat{b} + (i\Omega_r\hat{b}^\dagger + \mathrm{H.c.}). \quad (3)$$

The first term in Eq. (3) corresponds to a rotation of the amplitude α in the complex plane about the virtual origin α_{vo} with an angular frequency χ in a direction determined by the qubit state. Thus driving the qubit at the resonator frequency ω_r effectively shifts the origin of the resonator phase space to a point α_{vo} in the rotating frame.

The term $(\Omega_q + i\Omega_r\chi/g)\hat{\sigma}_+$ in Eq. (2) shows that the drives slightly tilt the qubit Hamiltonian. The tilt of the quantization axis determines the speed at which the drives

can be turned on while maintaining adiabaticity, the lowest-order condition being approximately $\dot{\Omega}_q \ll \Delta^2/\sqrt{2}$. Since $\Omega_q \ll \Delta$, the rise time of the qubit drive pulse can be negligibly short compared with the relevant dynamics of the resonator states. Thus, the qubit-state-dependent separation dynamics of the resonator state starts to take place essentially instantly in this readout protocol.

In contrast to the multichannel readout visualized in Fig. 1(c), the usual dispersive readout relies solely on the term $-\chi\hat{\sigma}_z\hat{a}^\dagger\hat{a}$, which implies that one needs to use the resonator drive to populate the resonator for the state separation to take place, see Fig. 1(b). The characteristic timescale for the population dynamics $1/\kappa$ is determined by the internal and external damping rates of the resonator κ_i and κ_x, respectively, as $\kappa = \kappa_i + \kappa_x$.

In addition to the potentially faster readout, our scheme offers more control over the evolution of the states than the usual dispersive readout. For example, we may continuously drive the resonator such that either α_e or α_g end in any desired position at the end of the readout. For example, choosing $i\Omega_r = \Omega_q\chi/g$ in Eq. (2) causes α_g to remain in vacuum while α_e is displaced. Interestingly, we may also reset the resonator to the vacuum state unconditionally on the qubit state and without feedback control. As illustrated in Fig. 1(c), one may shift the phase of α_{vo} by π after the actual measurement pulse and wait for both of the amplitudes α_e and α_g to rotate on top of each other. Subsequently, both distributions may be shifted to the vacuum state using a single pulse on the resonator.

Note that due to the finite resonator bandwidth, the resonator will slowly saturate towards a steady state. We obtain the steady states by solving the standard Lindblad master equation $\dot{\hat{\rho}} = -i[\hat{H},\hat{\rho}]/\hbar + \kappa\mathcal{L}[\hat{a}]\hat{\rho}/2$, where $\mathcal{L}[\hat{a}]$ is the Lindblad superoperator and $\hat{\rho}$ is the density operator of the qubit-resonator system. Forcing the states to remain coherent, the steady states $|\alpha^s_{g/e}\rangle$ are given by $\alpha^s_{g/e} = (i\Omega_r \mp \Omega_q\chi/g)/(i\kappa/2 \pm \chi)$. Above, we have restricted our theory to the case of a two-level system. However, the scheme also works in the case of many nonequidistant levels [48] such as those of a superconducting transmon qubit [58] studied below. Here, the driving frequency needs to be slightly offset from that of the resonator and an additional resonator drive is needed to obtain essentially Eq. (2) for the transmon. Note that qubit nonlinearity is pivotal to obtain a nonvanishing dispersive shift χ.

To implement our theoretical scheme we have fabricated [48] a superconducting Xmon qubit [59] shown in Fig. 2(a). It is coupled with strength $g = 2\pi \times 130$ MHz to a coplanar waveguide resonator of frequency $\omega_r/2\pi = 6.02$ GHz. The resonator has internal and external loss rates $\kappa_i = 2\pi \times 0.5$ and $\kappa_x = 2\pi \times 1.5$ MHz, respectively. We tune the qubit to the point of optimal phase coherence [48], $\omega_q/2\pi = 7.86$ GHz, where it is characterized by the energy relaxation

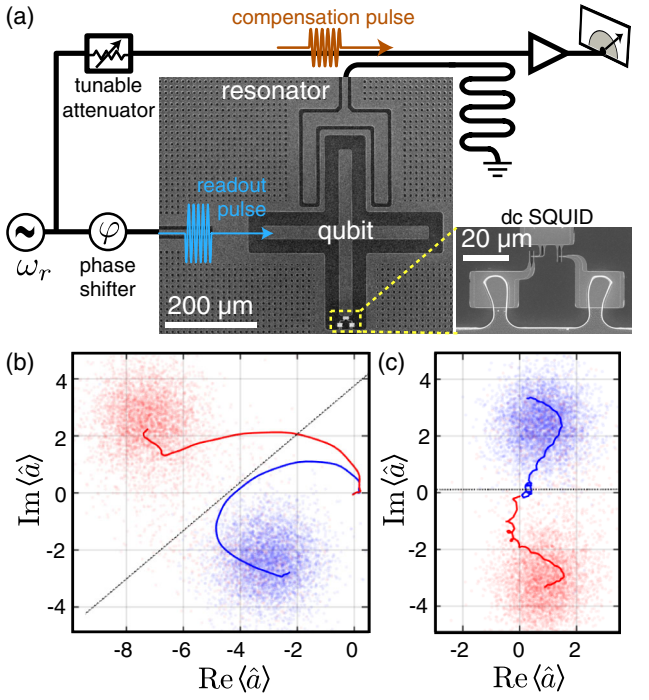

FIG. 2. (a) Simplified measurement setup and scanning electron micrographs of the experimental sample realizing the theoretical scheme. We employ an Xmon qubit [59], the frequency of which may be tuned by applying an external magnetic flux to the accompanying dc SQUID. The qubit is capacitively coupled to a voltage drive line and to a coplanar waveguide resonator which is, in turn, coupled to a transmission line. After amplification, we measure the two quadratures $\mathrm{Re}\,\hat{a}$ and $\mathrm{Im}\,\hat{a}$ of the resonator field. (b) Evolution of the amplitudes of the coherent states corresponding to the ground (blue line) and excited (red line) states of the qubit during a 420-ns conventional dispersive readout. Corresponding results of single-shot measurements are shown by dots (see text for details). The dotted line indicates the threshold for assigning the measurement outcome. (c) As (b), but the drive tone is applied to both the qubit and the resonator with an optimized relative phase. The single-shot measurement fidelities are 96.4% and 96.6% for (b) and (c), respectively.

time $T_1 = 3.0\ \mu$s. This leads to a dispersive shift $\chi = -2\pi \times 1.6$ MHz. We mount the sample to the base temperature stage, $T = 20$ mK, of a dilution refrigerator and extract the effective qubit temperature $T_{\mathrm{eff}} = 73$ mK from histograms of single-shot measurements [48]. For this purpose, we use a traveling-wave parametric amplifier [60] and a heterodyne detection setup to measure the two quadratures $\mathrm{Re}\,\hat{a}$ and $\mathrm{Im}\,\hat{a}$ of the resonator field.

Figures 2(b) and 2(c) present the experimentally measured temporal trajectories of ensemble-averaged expectation values $\alpha(t) = \langle\hat{a}(t)\rangle$ for the conventional readout and our method, respectively. The trajectories show qualitative agreement with our theory: In the conventional readout, the states move in the general direction of the drive and separate as the distance to the origin increases. In our scheme, the states move to opposite directions owing

to precession about the virtual origin lying on the negative real axis. The dominating differences between Figs. 1(b), 1(c) and 2(b), 2(c) can be explained by the higher levels of the transmon [48].

To characterize the performance of our method, we implement single-shot measurements S, of the observable $\hat{S} = \int_0^\tau [W_{\mathrm{Re}}(t)\mathrm{Re}\,\hat{a}(t) + iW_{\mathrm{Im}}(t)\mathrm{Im}\,\hat{a}(t)]dt$ by temporal integration of the readout signal. Here, the normalized weight functions are determined from the previously measured trajectories as $W_{\mathrm{Re}}(t) \propto |\mathrm{Re}[\alpha_e(t) - \alpha_g(t)]|$ and $W_{\mathrm{Im}}(t) \propto |\mathrm{Im}[\alpha_e(t) - \alpha_g(t)]|$. Thus the most weight is given to the signal when the state separation is known to be the largest. We also determine reference points α_j^{ref} by averaging shots conditioned on the qubit being in state $j \in \{g, e\}$. For a single measurement shot S, we infer that the qubit was in state $|g\rangle$ if $|S - \alpha_g^{\mathrm{ref}}| < |S - \alpha_e^{\mathrm{ref}}|$, see Figs. 2(b) and 2(c).

The error probability of assigning an incorrect label for the intended qubit state is calculated as $\epsilon_{\mathrm{total}} = [p(e|g) + p(g|e)]/2$, where $p(j|k)$ is the sampled probability to assign the label j to a state supposedly prepared in $|k\rangle$. To extract the error due to readout, we independently measure the state preparation errors caused by faulty gate operations, spontaneous decay, and thermal excitation. We estimate that these sources account for $\epsilon_{\mathrm{prep}} = 2.6\%$ of the total error, mainly limited by T_1 decay of our sample (see Ref. [48] for details).

We benchmark the speed and fidelity of our readout scheme against the conventional method in Fig. 3, which demonstrates that driving the qubit directly, with or without the compensation tone on the resonator, yields considerably lower errors for integration times $\tau \leq 350$ ns. Thus, measuring the qubit state by direct or multichannel driving results in a noticeable speedup over driving only the resonator. For each readout scheme, the drive power is independently maximized with the condition that the third level of the transmon is negligibly excited during readout, to ensure that the readout realizes a non-demolition measurement. For the multichannel readout, the relative phase between the resonator and qubit drives $\phi_r - \phi_q$ is also optimized to achieve the fastest decrease in error. We observe that for a given integration time, the conventional readout bears close to 100% larger measurement error than the multichannel driving scheme.

Combining the two drive channels provides versatile tools for controlling the state of the resonator. In Fig. 4(a), we show that as a function of the phase ϕ_q, the steady states draw circles in the complex plane, the centers and radii of which depend on the qubit state. This behavior is in agreement with the above result $\alpha_{g/e}^s = (i\Omega_r \mp \Omega_q\chi/g)/(i\kappa/2 \pm \chi)$. It appears possible to choose the phase of Ω_q such that the resonator state corresponding to one of the qubit states remains in the vacuum state (gray arrows), a situation inaccessible by driving only the resonator. In

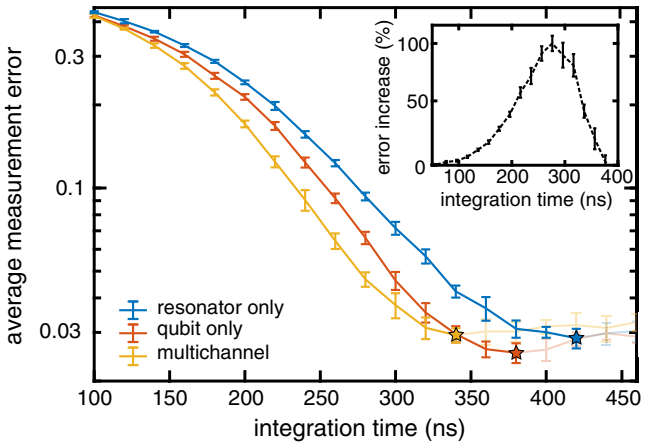

FIG. 3. Average measurement error $\epsilon_{\mathrm{total}} - \epsilon_{\mathrm{prep}}$ as a function of integration time for the conventional readout (blue markers), qubit driving (red markers), and multichannel driving (yellow markers). Each data point shows the average and the standard deviation of 10 measurement runs consisting of 10^4 single-shot measurements. The stars indicate the time for which the lowest error is obtained for each method. The inset shows the relative increase in the measurement error when the readout method is changed from the multichannel scheme to the conventional readout. When we drive the resonator only, the experimental parameters are identical to those in Fig. 2(b) and with multichannel driving to those in Fig. 2(c). For the multichannel readout, the drive powers to the resonator and to the qubit are decreased by 2 and 1 dB compared with single-channel driving, respectively.

Fig. 4(b), we show that with the multichannel method we can indeed leave α_g near the origin while significantly displacing α_e. As discussed above, a related mechanism may be utilized to unconditionally reset the resonator after

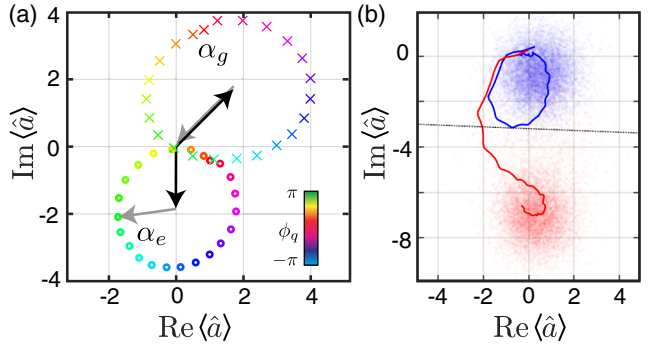

FIG. 4. (a) Measured means of the steady states corresponding to $|g\rangle$ (α_g) and $|e\rangle$ (α_e) in the multichannel readout as functions of the phase ϕ_q of the qubit drive pulse, as indicated by the different colors of the markers. The black arrows denote phase-independent contributions to the steady state owing to the resonator drive. With a particular choice of ϕ_q, indicated by the gray arrows, one of the resonator states returns to vacuum during the measurement. (b) Evolution of the amplitude of the coherent state (solid lines) for qubit ground (blue color) and excited (red color) states in the partial reset scheme. The phase ϕ_q is chosen such that the steady state for $|g\rangle$ lies at the origin.

the readout to further reduce the duration of the overall measurement protocol.

In conclusion, we have proposed and experimentally demonstrated a readout scheme for a qubit dispersively coupled to a bosonic mode. By driving both the qubit and the mode close to the mode frequency, the readout can be turned on much faster than any other relevant timescale in the system and the resonator can be unconditionally brought back to the vacuum state without the need for feedback control. Our experiments with a superconducting qubit demonstrate resonator control through the qubit. For a given readout time in our sample, we experimentally observe that the conventional readout may lead to more than 100% larger error than that of the proposed scheme.

In the future, we aim to realize the unconditional reset protocol and to optimize the sample design such that we improve on the present state-of-the-art readout [26]. Furthermore, our proposal could be implemented in a variety of systems such as qubits coupled to nanomechanical resonators [35,36]. We expect that in addition to qubit readout, an extension of our protocol may also be beneficial for resonator state control such as the creation of cat states [61].

We acknowledge William Oliver, Greg Calusine, Kevin O'Brien, and Irfan Siddiqi for providing us with the traveling-wave parametric amplifier used in the experiments. This research was financially supported by European Research Council under Grant No. 681311 (QUESS) and Marie Skłodowska-Curie Grant No. 795159; by Academy of Finland under its Centres of Excellence Program Grants No. 312300 and No 312059 and under other Grants No. 265675, No. 305237, No. 305306, No. 308161, No. 312300, No. 314302, No. 316551, and No. 319579; Finnish Cultural Foundation, the Jane and Aatos Erkko Foundation, Vilho, Yrjö and Kalle Väisälä Foundation, and the Technology Industries of Finland Centennial Foundation. We thank the provision of facilities and technical support by Aalto University at OtaNano–Micronova Nanofabrication Centre.

Note added.—Recently, Ref. [62] pursuing a similar readout scheme came to our attention. Our work is fully independent of this reference.

[1] A. Bassi, K. Lochan, S. Satin, T. P. Singh, and H. Ulbricht, Models of wave-function collapse, underlying theories, and experimental tests, Rev. Mod. Phys. **85**, 471 (2013).

[2] M. Fuwa, S. Takeda, M. Zwierz, H. M. Wiseman, and A. Furusawa, Experimental proof of nonlocal wavefunction collapse for a single particle using homodyne measurements, Nat. Commun. **6**, 6665 (2015).

[3] B. S. DeWitt and N. Graham, *The Many Worlds Interpretation of Quantum Mechanics* (Princeton University Press, Princeton, 2015).

[4] J. L. O'Brien, A. Furusawa, and J. Vučković, Photonic quantum technologies, Nat. Photonics **3**, 687 (2009).

[5] T. D. Ladd, F. Jelezko, R. Laflamme, Y. Nakamura, C. Monroe, and J. L. O'Brien, Quantum computers, Nature (London) **464**, 45 (2010).

[6] G. Kurizki, P. Bertet, Y. Kubo, K. Mølmer, D. Petrosyan, P. Rabl, and J. Schmiedmayer, Quantum technologies with hybrid systems, Proc. Natl. Acad. Sci. U.S.A. **112**, 3866 (2015).

[7] D. Ristè, S. Poletto, M.-Z. Huang, A. Bruno, V. Vesterinen, O.-P. Saira, and L. DiCarlo, Detecting bit-flip errors in a logical qubit using stabilizer measurements, Nat. Commun. **6**, 6983 (2015).

[8] J. Kelly *et al.*, State preservation by repetitive error detection in a superconducting quantum circuit, Nature (London) **519**, 66 (2015).

[9] S. Hacohen-Gourgy, L. S. Martin, E. Flurin, V. V. Ramasesh, K. B. Whaley, and I. Siddiqi, Quantum dynamics of simultaneously measured non-commuting observables, Nature (London) **538**, 491 (2016).

[10] M. Reagor *et al.*, Demonstration of universal parametric entangling gates on a multi-qubit lattice, Sci. Adv. **4**, eaao3603 (2018).

[11] A. G. Fowler, A. M. Stephens, and P. Groszkowski, High-threshold universal quantum computation on the surface code, Phys. Rev. A **80**, 052312 (2009).

[12] A. G. Fowler, Two-dimensional color-code quantum computation, Phys. Rev. A **83**, 042310 (2011).

[13] D. Ristè, M. Dukalski, C. A. Watson, G. de Lange, M. J. Tiggelman, Y. M. Blanter, K. W. Lehnert, R. N. Schouten, and L. DiCarlo, Deterministic entanglement of superconducting qubits by parity measurement and feedback, Nature (London) **502**, 350 (2013).

[14] R. Barends, J. Kelly, A. Megrant, A. Veitia, D. Sank, E. Jeffrey, T. C. White, J. Mutus, A. G. Fowler, B. Campbell, Y. Chen, Z. Chen, B. Chiaro, A. Dunsworth, C. Neill, P. O'Malley, P. Roushan, A. Vainsencher, J. Wenner, A. N. Korotkov, A. N. Cleland, and J. M. Martinis, Superconducting quantum circuits at the surface code threshold for fault tolerance, Nature (London) **508**, 500 (2014).

[15] D. Nigg, M. Müller, E. A. Martinez, P. Schindler, M. Hennrich, T. Monz, M. A. Martin-Delgado, and R. Blatt, Quantum computations on a topologically encoded qubit, Science, **345** 302 (2014).

[16] K. Geerlings, Z. Leghtas, I. M. Pop, S. Shankar, L. Frunzio, R. J. Schoelkopf, M. Mirrahimi, and M. H. Devoret, Demonstrating a Driven Reset Protocol for a Superconducting Qubit, Phys. Rev. Lett. **110**, 120501 (2013).

[17] C. C. Bultink, M. A. Rol, T. E. O'Brien, X. Fu, B. C. S. Dikken, C. Dickel, R. F. L. Vermeulen, J. C. de Sterke, A. Bruno, R. N. Schouten, and L. DiCarlo, Active Resonator Reset in the Nonlinear Dispersive Regime of Circuit QED, Phys. Rev. Applied **6**, 034008 (2016).

[18] P. Magnard, P. Kurpiers, B. Royer, T. Walter, J.-C. Besse, S. Gasparinetti, M. Pechal, J. Heinsoo, S. Storz, A. Blais, and A. Wallraff, Fast and Unconditional All-Microwave Reset of a Superconducting Qubit, Phys. Rev. Lett. **121**, 060502 (2018).

[19] E. Knill, R. Laflamme, and G. J. Milburn, A scheme for efficient quantum computation with linear optics, Nature (London) **409**, 46 (2001).

[20] M. A. Nielsen, Optical Quantum Computation Using Cluster States, Phys. Rev. Lett. **93**, 040503 (2004).
[21] P. Kok, W. J. Munro, K. Nemoto, T. C. Ralph, J. P. Dowling, and G. J. Milburn, Linear optical quantum computing with photonic qubits, Rev. Mod. Phys. **79**, 135 (2007).
[22] J. Gambetta, W. A. Braff, A. Wallraff, S. M. Girvin, and R. J. Schoelkopf, Protocols for optimal readout of qubits using a continuous quantum nondemolition measurement, Phys. Rev. A **76**, 012325 (2007).
[23] D. Ristè, C. C. Bultink, K. W. Lehnert, and L. DiCarlo, Feedback Control of a Solid-State Qubit Using High-Fidelity Projective Measurement, Phys. Rev. Lett. **109**, 240502 (2012).
[24] E. Jeffrey, D. Sank, J. Y. Mutus, T. C. White, J. Kelly, R. Barends, Y. Chen, Z. Chen, B. Chiaro, A. Dunsworth, A. Megrant, P. J. J. O'Malley, C. Neill, P. Roushan, A. Vainsencher, J. Wenner, A. N. Cleland, and J. M. Martinis, Fast Accurate State Measurement with Superconducting Qubits, Phys. Rev. Lett. **112**, 190504 (2014).
[25] J. Goetz, S. Pogorzalek, F. Deppe, K. G. Fedorov, P. Eder, M. Fischer, F. Wulschner, E. Xie, A. Marx, and R. Gross, Photon Statistics of Propagating Thermal Microwaves, Phys. Rev. Lett. **118**, 103602 (2017).
[26] T. Walter, P. Kurpiers, S. Gasparinetti, P. Magnard, A. Potočnik, Y. Salathé, M. Pechal, M. Mondal, M. Oppliger, C. Eichler, and A. Wallraff, Rapid High-Fidelity Single-Shot Dispersive Readout of Superconducting Qubits, Phys. Rev. Applied **7**, 054020 (2017).
[27] S. J. Weber, G. O. Samach, D. Hover, S. Gustavsson, D. K. Kim, A. Melville, D. Rosenberg, A. P. Sears, F. Yan, J. L. Yoder, W. D. Oliver, and A. J. Kerman, Coherent Coupled Qubits for Quantum Annealing, Phys. Rev. Applied **8**, 014004 (2017).
[28] S. Rosenblum, P. Reinhold, M. Mirrahimi, L. Jiang, L. Frunzio, and R. J. Schoelkopf, Fault-tolerant detection of a quantum error, Science **361**, 266 (2018).
[29] J. I. Colless, A. C. Mahoney, J. M. Hornibrook, A. C. Doherty, H. Lu, A. C. Gossard, and D. J. Reilly, Dispersive Readout of a Few-Electron Double Quantum Dot with Fast rf Gate Sensors, Phys. Rev. Lett. **110**, 046805 (2013).
[30] P. Scarlino, D. J. van Woerkom, A. Stockklauser, J. V. Koski, M. C. Collodo, S. Gasparinetti, C. Reichl, W. Wegscheider, T. Ihn, K. Ensslin, and A. Wallraff, All-Microwave Control and Dispersive Readout of Gate-Defined Quantum Dot Qubits in Circuit Quantum Electrodynamics, arXiv:1711.01906.
[31] X. Mi, C. G. Péterfalvi, G. Burkard, and J. R. Petta, High-Resolution Valley Spectroscopy of Si Quantum Dots, Phys. Rev. Lett. **119**, 176803 (2017).
[32] R. Blatt and C. F. Roos, Quantum simulations with trapped ions, Nat. Phys. **8**, 277 (2012).
[33] A. Blais, R.-S. Huang, A. Wallraff, S. M. Girvin, and R. J. Schoelkopf, Cavity quantum electrodynamics for superconducting electrical circuits: An architecture for quantum computation, Phys. Rev. A **69**, 062320 (2004).
[34] A. Wallraff, D. I. Schuster, A. Blais, L. Frunzio, R.-S. Huang, J. Majer, S. Kumar, S. M. Girvin, and R. J. Schoelkopf, Strong coupling of a single photon to a superconducting qubit using circuit quantum electrodynamics, Nature (London) **431**, 162 (2004).
[35] J. Bochmann, A. Vainsencher, D. D. Awschalom, and A. N. Cleland, Nanomechanical coupling between microwave and optical photons, Nat. Phys. **9**, 712 (2013).
[36] J.-M. Pirkkalainen, S. U. Cho, J. Li, G. S. Paraoanu, P. J. Hakonen, and M. A. Sillanpää, Hybrid circuit cavity quantum electrodynamics with a micromechanical resonator, Nature (London) **494**, 211 (2013).
[37] Y. Tabuchi, S. Ishino, A. Noguchi, T. Ishikawa, R. Yamazaki, K. Usami, and Y. Nakamura, Coherent coupling between a ferromagnetic magnon and a superconducting qubit, Science, **349**, 405 (2015).
[38] E. Jaynes and F. Cummings, Comparison of quantum and semiclassical radiation theories with application to the beam maser, Proc. IEEE **51**, 89 (1963).
[39] B. W. Shore and P. L. Knight, The Jaynes-Cummings Model, J. Mod. Opt. **40**, 1195 (1993).
[40] A. Wallraff, D. I. Schuster, A. Blais, L. Frunzio, J. Majer, M. H. Devoret, S. M. Girvin, and R. J. Schoelkopf, Approaching Unit Visibility for Control of a Superconducting Qubit with Dispersive Readout, Phys. Rev. Lett. **95**, 060501 (2005).
[41] F. Mallet, F. R. Ong, A. Palacios-Laloy, F. Nguyen, P. Bertet, D. Vion, and D. Esteve, Single-shot qubit readout in circuit quantum electrodynamics, Nat. Phys. **5**, 791 (2009).
[42] M. Jerger, S. Poletto, P. Macha, U. Hübner, E. Il'ichev, and A. V. Ustinov, Frequency division multiplexing readout and simultaneous manipulation of an array of flux qubits, Appl. Phys. Lett. **101**, 042604 (2012).
[43] J. Heinsoo, C. K. Andersen, A. Remm, S. Krinner, T. Walter, Y. Salathé, S. Gasparinetti, J.-C. Besse, A. Potočnik, A. Wallraff, and C. Eichler, Rapid High-fidelity Multiplexed Readout of Superconducting Qubits, Phys. Rev. Applied **10**, 034040 (2018).
[44] D. T. McClure, H. Paik, L. S. Bishop, M. Steffen, J. M. Chow, and J. M. Gambetta, Rapid Driven Reset of a Qubit Readout Resonator, Phys. Rev. Applied **5**, 011001 (2016).
[45] N. T. Bronn, Y. Liu, J. B. Hertzberg, A. D. Crcoles, A. A. Houck, J. M. Gambetta, and J. M. Chow, Broadband filters for abatement of spontaneous emission in circuit quantum electrodynamics, Appl. Phys. Lett. **107**, 172601 (2015).
[46] J. Ikonen and M. Möttönen, Accelerated stabilization of coherent photon states, New J. Phys., **20**, 103047 (2018).
[47] M. Boissonneault, J. M. Gambetta, and A. Blais, Dispersive regime of circuit QED: Photon-dependent qubit dephasing and relaxation rates, Phys. Rev. A **79**, 013819 (2009).
[48] See Supplemental Material at http://link.aps.org/supplemental/10.1103/PhysRevLett.122.080503 for experimental techniques and theoretical derivations, which include Refs. [49–55].
[49] J. M. Sage, V. Bolkhovsky, W. D. Oliver, B. Turek, and P. B. Welander, Study of loss in superconducting coplanar waveguide resonators, J. Appl. Phys. **109**, 063915 (2011).
[50] G. J. Dolan, Offset masks for lift-off photoprocessing, Appl. Phys. Lett. **31**, 337 (1977).
[51] J. Goetz, F. Deppe, M. Haeberlein, F. Wulschner, C. W. Zollitsch, S. Meier, M. Fischer, P. Eder, E. Xie, K. G. Fedorov, E. P. Menzel, A. Marx, and R. Gross, Loss mechanisms in superconducting thin film microwave resonators, J. Appl. Phys. **119**, 015304 (2016).

[52] J. Goetz, F. Deppe, P. Eder, M. Fischer, M. Müting, J. Puertas Martínez, S. Pogorzalek, F. Wulschner, E. Xie, K. G. Fedorov, A. Marx, and R. Gross, Second-order decoherence mechanisms of a transmon qubit probed with thermal microwave states, Quant. Sci. Technol. **2**, 025002 (2017).

[53] A. Megrant, C. Neill, R. Barends, B. Chiaro, Y. Chen, L. Feigl, J. Kelly, E. Lucero, M. Mariantoni, P. O'Malley, D. Sank, A. Vainsencher, J. Wenner, T. White, Y. Yin, J. Zhao, C. Palmström, J. M. Martinis, and A. Cleland, Planar superconducting resonators with internal quality factors above one million, Appl. Phys. Lett. **100**, 113510 (2012).

[54] E. Magesan, J. M. Gambetta, and J. Emerson, Characterizing quantum gates via randomized benchmarking, Phys. Rev. A **85**, 042311 (2012).

[55] J. M. Epstein, A. W. Cross, E. Magesan, and J. M. Gambetta, Investigating the limits of randomized benchmarking protocols, Phys. Rev. A **89**, 062321 (2014).

[56] N. Didier, J. Bourassa, and A. Blais, Fast Quantum Nondemolition Readout by Parametric Modulation of Longitudinal Qubit-Oscillator Interaction, Phys. Rev. Lett. **115**, 203601 (2015).

[57] P.-M. Billangeon, J. S. Tsai, and Y. Nakamura, Circuit-QED-based scalable architectures for quantum information processing with superconducting qubits, Phys. Rev. B **91**, 094517 (2015).

[58] J. Koch, T. M. Yu, J. Gambetta, A. A. Houck, D. I. Schuster, J. Majer, A. Blais, M. H. Devoret, S. M. Girvin, and R. J. Schoelkopf, Charge-insensitive qubit design derived from the Cooper pair box, Phys. Rev. A **76**, 042319 (2007).

[59] R. Barends, J. Kelly, A. Megrant, D. Sank, E. Jeffrey, Y. Chen, Y. Yin, B. Chiaro, J. Mutus, C. Neill, P. O'Malley, P. Roushan, J. Wenner, T. C. White, A. N. Cleland, and J. M. Martinis, Coherent Josephson Qubit Suitable for Scalable Quantum Integrated Circuits, Phys. Rev. Lett. **111**, 080502 (2013).

[60] C. Macklin, K. O'Brien, D. Hover, M. E. Schwartz, V. Bolkhovsky, X. Zhang, W. D. Oliver, and I. Siddiqi, A near–quantum-limited Josephson traveling-wave parametric amplifier, Science **350**, 307 (2015).

[61] B. Vlastakis, G. Kirchmair, Z. Leghtas, S. E. Nigg, L. Frunzio, S. M. Girvin, M. Mirrahimi, M. H. Devoret, and R. J. Schoelkopf, Deterministically encoding quantum information using 100-photon schrödinger cat states, Science **342**, 607 (2013).

[62] S. Touzard, A. Kou, N. Frattini, V. Sivak, S. Puri, A. Grimm, L. Frunzio, S. Shankar, and M. Devoret, preceding Letter, Gated Conditional Displacement Readout of Superconducting Qubits, Phys. Rev. Lett. **122**, 080502 (2018).